localize fungal endophytes. *Int. J. Pharm. Sci. Rev. Res*., 2013, **20**, 205–209.
9. Sun, B. Da., Chen, A. J., Gao, W. W., Zhou, Y. G. and Liu, H. Y., Endophytic fungi associated with the medicinal plant, *Achyranthes bidentata* Blume (Amaranthaceae). *Afr. J. Microbiol. Res*., 2003, **15**, 1357–1365.
10. Tian, W., Bi, Y. H., Zeng, W., Jiang, W., Xue, Y. H., Wang, G. X. and Liu, S. P., Diversity of endophytic fungi of *Myricaria laxiflora* grown under pre- and post-flooding conditions. *Genet. Mol. Res*., 2015, **14**, 10849–10862.
11. Doley, P. and Jha, D. K., Endophytic fungal assemblages from ethnomedicinal plant *Rauwolfia serpentina* (L) Benth. *J. Plant Pathol. Microbiol*., 2010, **40**, 44–48.
12. Gangwar, A. K. and Ghosh, A. K., Medicinal uses and pharmacological activity of *Adhatoda vasica*. *Int. J. Herbal Med*., 2014, **2**, 88–91.
13. Singh, T. P., Singh, O. M. and Singh, H. B., *Adhatoda vasica* Nees: phytochemical and pharmacological profile. *Nat. Prod. J*., 2011, **1**, 29–39.
14. Pandita, K., Bhatia, M. S., Thappa, R. K., Agarwal, S. G., Dhar, K. L. and Atal, C. K., Seasonal variation of alkaloids of *Adhatoda vasica* and detection of glycosides and N-oxides of vasicine and vasicinone. *Planta Med*., 1983, **48**, 81–82.
15. Claeson, U. P., Malmfors, T., Wikman, G. and Bruhn, J. G., *Adhatoda vasica*: a critical review of ethnopharmacological and toxicological data. *J. Ethnopharmacol*., 2000, **72**, 1–20.
16. Mishra, Y., Singh, A., Batra, A. and Sharma, M. M., Understanding the biodiversity and biological applications of endophytic fungi: a review. *J. Microb. Biochem. Technol*., 2014, **8**, 1–11.
17. Johansen, D. A., *Plant Microtechnique*, McGraw-Hill, New York, 1940, p. 523.
18. Schichnes, D., Nemson, J. A. and Ruzin, S. E., Microwave paraffin techniques for botanical tissues. In *Microwave Techniques and Protocols* (eds Giberson R. T. and Demaree, R. S.), Humana Press, New Jersey, 2001, pp. 181–189.
19. Verma, V. C., Singh, S. K. and Kharwar, R. N., Histological investigation of fungal endophytes in healthy tissues of *Azadirachta indica*. A. Juss. *Kasetsart J. Nat. Sci*., 2012, **46**, 229–237.
20. Behie, S. W., Jones, S. J. and Bidochka, M. J., Plant tissue localization of the endophytic insect pathogenic fungi *Metarhizium* and *Beauveria*. *Fungal Ecol*., 2015, **13**, 112–119.
21. Salgado, S. C., Cepero, M. C., Realpe, E. and Restrepo, S., Histological analyses of the fungal endophytes in Rosa hybrid. *Rev. Iberoam. Micol*., 2007, **24**, 323–324.
22. Wang, Y., Guo, L.-D. and Hyde, K. D., Taxonomic placement of sterile morphotypes of endophytic fungi from *Pinus tabulaeformis* (Pinaceae) in northeast China based on rDNA sequences. *Fungal Divers*., 2005, **20**, 235–260.
23. Mishra, A., Gond, S. K., Kumar, A., Sharma, V. K., Verma, S. K., Kharwar, R. N. and Sieber, T. N., Season and tissue type affect fungal endophyte communities of the Indian medicinal plant *Tinospora cordifolia* more strongly than geographic location. *Microb. Ecol.*, 2012, **64**, 388–398.
24. Kharwar, R. N. *et al.*, Diversity and biopotential of endophytic fungal flora isolated from eight medicinal plants of Uttar Pradesh, India. In *Microbial Diversity and Biotechnology in Food Security* (eds Kharwar R. N. *et al.*), Springer, India, 2014, pp. 23–39.

ACKNOWLEDGEMENT. We thank Prof. Sandeep Sancheti, President Manipal University, Jaipur for providing the necessary laboratory facilities.

Received 9 November 2015; revised accepted 23 November 2016

doi: 10.18520/cs/v112/i10/2112-2115

Seasonal variation in nearshore wave characteristics off Cuddalore, Southeast coast of Tamil Nadu, India

Basanta Kumar Jena*, Sisir K. Patra, K. Jossia Joseph and K. M. Sivakholundu

Coastal and Environmental Engineering Division,
National Institute of Ocean Technology, Pallikaranai,
Chennai 600 100, India

Wave data collected using wave rider buoy between January 2010 and January 2011 off Cuddalore coast, Tamil Nadu, India, have been analysed season-wise in this study. Wave steepness method was used for the separation of sea and swell wave parameters. Also parameters such as significant wave height of total wave, sea and swell (H_s, H_{sw} and H_{ss}), zero crossing periods (T_z, T_{sw} and T_{ss}) and mean wave directions (θ, θ_{sw} and θ_{ss}) have been studied. The study shows a distinct shift in sea wave direction of about 90° between June and October as well as November and February. Throughout the year, the predominant swell direction remained around 135°. The contribution in total H_s by H_{sw} was 76% and the remaining 24% by H_{ss} in the yearly cycle. The sea wave height was dominant by more than 90% during November to May. Regression analysis showed good positive Pearson's correlation of 0.94 between H_s and H_{sw}; however, it was 0.65 between H_s and H_{ss}. The maximum and significant wave heights of 5.7 and 2.7 m were recorded during cyclone *Jal* on 7 November 2010.

Keywords: Regression analysis, seasonal variation, spectral energy density, wave characteristics.

WAVE characteristics, viz. wave height, period, direction, energy of sea and swell play a crucial role in nearshore processes, planning and design of coastal structures, navigation and forecasting[1]. The wave and wave-dominated processes are the predominant factors for alteration of coastal geomorphology. Sea waves are generated by wind and as they propagate away from the generating area, they are called swell waves. Swell waves are known to travel long distances across the globe. Wind waves are generated locally and are strongly coupled to the local wind field, surpassing the contribution of tides, tsunamis and coastal surges[2]. Identification and separation of wave coagulations of wind sea and swell provide a more realistic depiction of the sea state and are of great importance to oceanography and engineering applications[3].

The wave climate of the seas around India varies from southwest monsoon (June–September) to northeast monsoon (October–January) and fair weather (February–May) period[4]. Seasonally, the wave climate can be subdivided

*For correspondence. (e-mail: bkjena@niot.res.in)

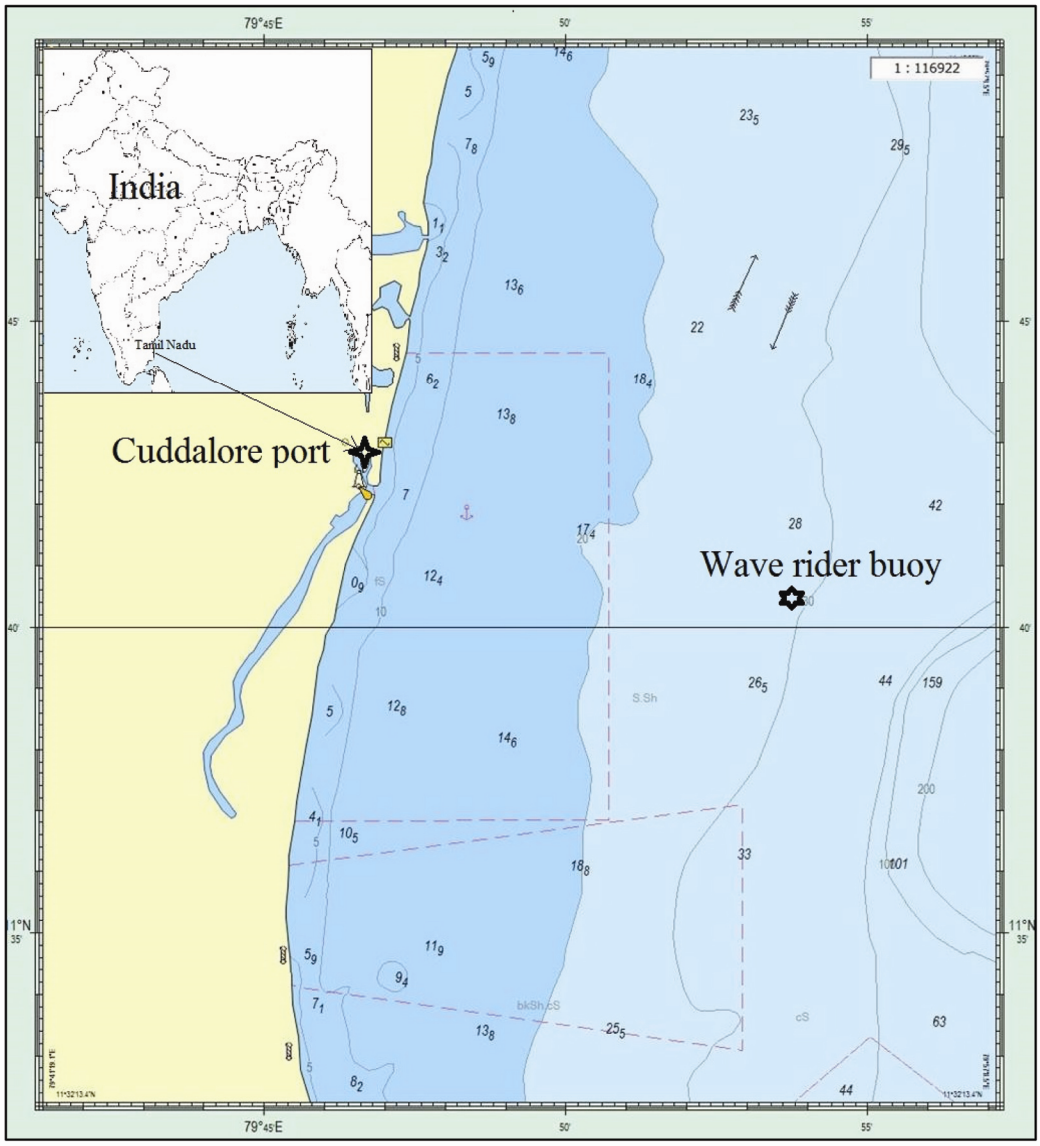

Figure 1. Map showing the study area and wave buoy deployment location.

into four categories: i.e. (i) high energy waves that occur during June to September; (ii) moderate energy waves during October and November; (iii) low energy waves during March to May and (iv) very low energy waves during December to February[5]. Long-period waves are observed mostly during the SW monsoon and are negligible during the NE monsoon period[6]. Conditions that prevail in the Arabian Sea are different from the present study location. Hence, it is better to describe the characteristics of waves off the Bay of Bengal (BoB). The southwestern BoB is a shadow area with relatively low wave height compared to the northern BoB[6]. The wave characteristics in the northern BoB are influenced by the SW and NE monsoons[7]. Due to locally generated waves, sea-dominated double-peaked wave spectra are observed during June to September compared with other periods[8]. In general, the wave spectra are double or multi-peaked in BoB[9], due to existence of seas along with swells. The single-peaked spectra are observed during cyclone events, and the peak of the wave spectral energy is concentrated in the low frequency region[5]. Many researchers have studied the sea and swell characteristics and their seasonal variability in the recent past, along the east coast of India[7,9–11]. In an earlier study, it has been reported that the contribution of swells to the total wave height was 63%, during the SW monsoon along Visakhapatnam, east coast of India[10]. Along the west coast of India (off Goa), the dominance of swell during SW monsoon, post-monsoon and pre-monsoon seasons is 93%, 67% and 49% respectively[12]. Information on the seasonal variability of the sea and swell along the east coast of India is limited. Hence in the present study, the sea and swell off

Table 1. Sampling frequency, resolution and accuracy of GPS buoy

Device parameters	Specifications
Sensor	GPS (not differential)
Approximate buoy weight, diameter and buoyancy	225 kg, 0.9 m and 1630 N
Sampling frequency	1.28 Hz
Sensor cut-off frequency/filtering type	0.01 Hz (using high-pass filter)/phase-linear, combined band-pass and single-integrating FIR type
Heave range, resolution and accuracy	–20 to +20 m, 1 cm and ± 1 cm or 0.1% of value
Wave direction range, resolution, accuracy and reference	0°–360°, 1.5°, 1.5° and true north
Wave period range	1.6–100 sec
Frequency range	0.025–0.60 Hz
HF transmission frequency and range	25.5–35.5 MHz and 50 km

Table 2. The maximum, minimum and average value of wave parameters for a period of one year (21 January 2010–20 January 2011)

Wave parameters	Minimum	Maximum	Average
Maximum wave height, H_{max} (m)	0.22	5.7	1.25
Significant wave height, H_s (m)	0.15	2.78	0.81
Significant sea wave height, H_{ss} (m)	0.05	2.21	0.67
Significant swell wave height, H_{sw} (m)	0.07	2.14	0.41
Peak wave period, T_p (sec)	2.1	20	8.6
Zero crossing sea wave period, T_z (sec)	2.29	6.27	3.7
Zero crossing swell wave period, T_{sw} (sec)	8.29	20.08	10.28
Zero crossing wave period, T_{ss} (sec)	2.56	9.52	4.46
Maximum spectral energy, E_{max} (m^2/Hz)	0.01	14.3	0.67

Cuddalore, Tamil Nadu, India have been separated from the measured wave spectra, and seasonal characteristic have been discussed.

Cuddalore is situated along the southeast coast of India with a shoreline orientation of approximately 20° with respect to north (Figure 1). The tide along this coast is semi-diurnal with maximum range of 1 m (ref. 13). The state Government has plans to develop an all-weather open seaport from the existing fair-weather port, through private sector participation. Therefore, the present study is useful to know the sea, swell and other wave characteristics for economic design of coastal structures (groyne, breaker water, pier, etc.), shoreline management planning and monitoring of future geo-morphological changes along Cuddalore coast.

Wave measurement was carried out at 30 m water depth using GPS (Global Positioning System; Datawell) based directional wave rider buoy, 12 km offshore from Cuddalore (11°40.7′N; 79°53′E). The data were collected for a period of one year between 21 January 2010 and 20 January 2011. The measurement principle of the GPS wave buoy is based on the Doppler shift phenomenon. The system calculates the velocity of the buoy from changes in the frequency received in the observed GPS signals[14]. The velocities are integrated with time to determine buoy displacement. In practice, the system uses signals from multiple satellites to determine three-dimensional buoy motions. In GPS buoy, data are sampled at a frequency of 1.28 Hz and measured velocities are digitally filtered using integrated high-pass filter with a cut-off frequency of 0.01 Hz. These velocities are converted into north–south, east–west and vertical motions at 1.28 Hz sample interval. Table 1 provides details of sampling frequency, resolution and accuracy of GPS buoy[14].

The separation of sea and swell components from the wave spectra was done by wave steepness method adopted by US National Data Buoy Center based on the wave frequency (f)[15]. Estimations were made by selecting a separation frequency f_s that partitions the wave spectrum into its sea and swell parts and their components, viz. significant wave height (H_{sw} and H_{ss}), zero crossing period (T_{sw} and T_{ss}) and mean wave direction (θ_{sw} and θ_{ss}). The steepness function $\xi(f)$ and separation frequency f_s are given by eqs (1) and (2).

$$\xi(f) = \frac{8\pi m_2(f)}{g\sqrt{m_0(f)}}, \tag{1}$$

$$f_s = Cf_m, \tag{2}$$

where f is the cyclic wave frequency, f_m the frequency of maximum $\xi(f)$, g the acceleration due to gravity, m_0 and m_2 are the zeroth- and second-order spectral moments, and $C = 0.75$ is an empirically determined constant[15].

Table 2 presents the maximum, minimum and average values of wave parameters. During the study period maximum wave height (H_{max}) of 5.7 m was recorded on

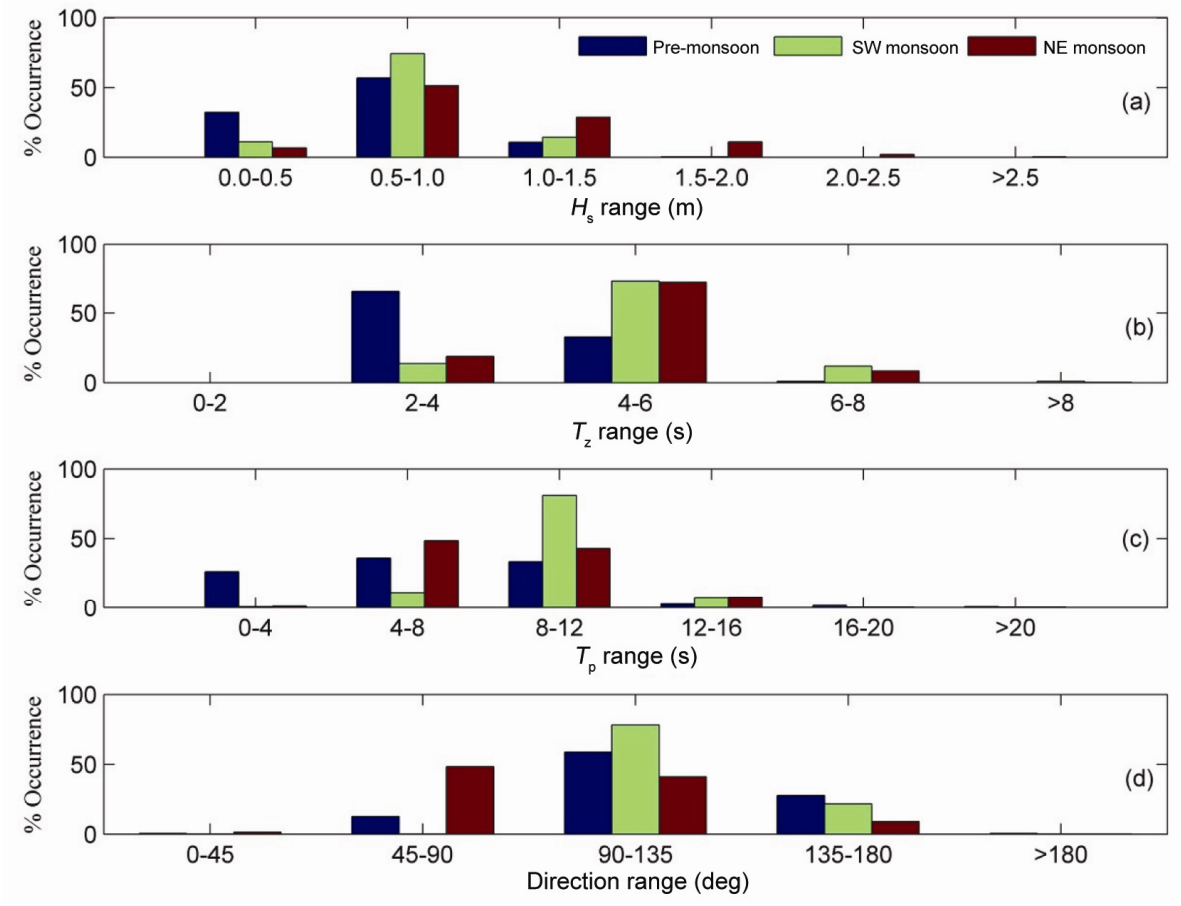

Figure 2. Percentage occurrence of H_s (significant wave height), T_z (zero crossing wave period), T_p (peak wave period) and direction.

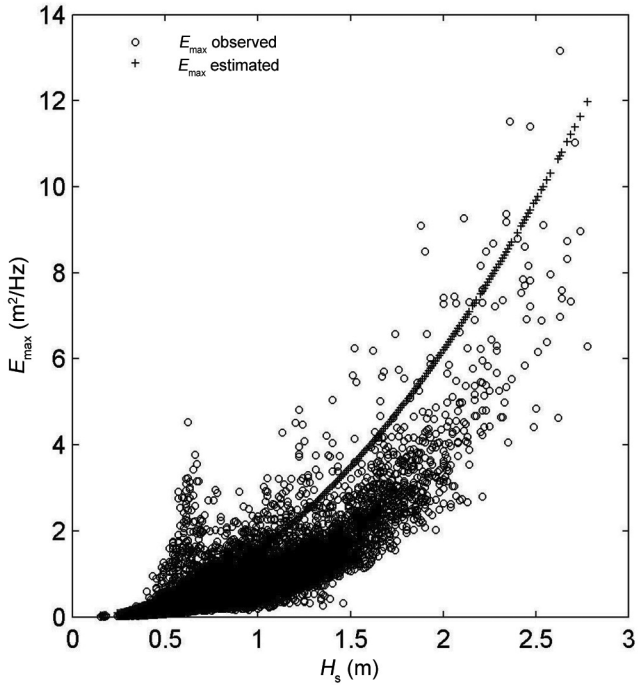

Figure 3. Variation of maximum spectral energy density (E_{max}) with significant wave height.

7 November 2010 during severe cyclone *Jal*. In addition to this, H_{max} also exceeded 4 m during May and October 2010 (during *Laila* and *Giri* cyclones), December 2010 and January 2011 (low pressure) events over BoB.

For a one-year period the significant wave height (H_s) ranged from 0.15 to 2.78 m with an average of 0.81 m; Table 2 shows the distribution. During pre-monsoon period, H_s ranged between 0.24 and 1.88 m with an average of 0.65 m; during southwest monsoon, it ranged between 0.15 and 1.62 m with an average of 0.76 m; and during NE monsoon H_s ranged between 0.25 and 2.78 m with an average of 1.01 m. The percentage distribution of significant wave height shows that during pre-monsoon months 32% of the wave is less than 0.5 m, 55% is in the range 0.5–1 m and the rest are more than 1 m (Figure 2). During SW monsoon, 74% of waves is between 0.5 and 1 m, about 15% is greater than 1 m and the rest less than 0.5 m. During NE monsoon, 51% of the waves range between 0.5 and 1 m; 29% between 1 and 1.5 m; 13% wave is more than 1.5 m; and 7% is less than 0.5 m. During the NE monsoon season, the wave intensity is more due to cyclone and depression formation in BoB and maximum value of H_s exceeding 2 m is observed mostly during October to January.

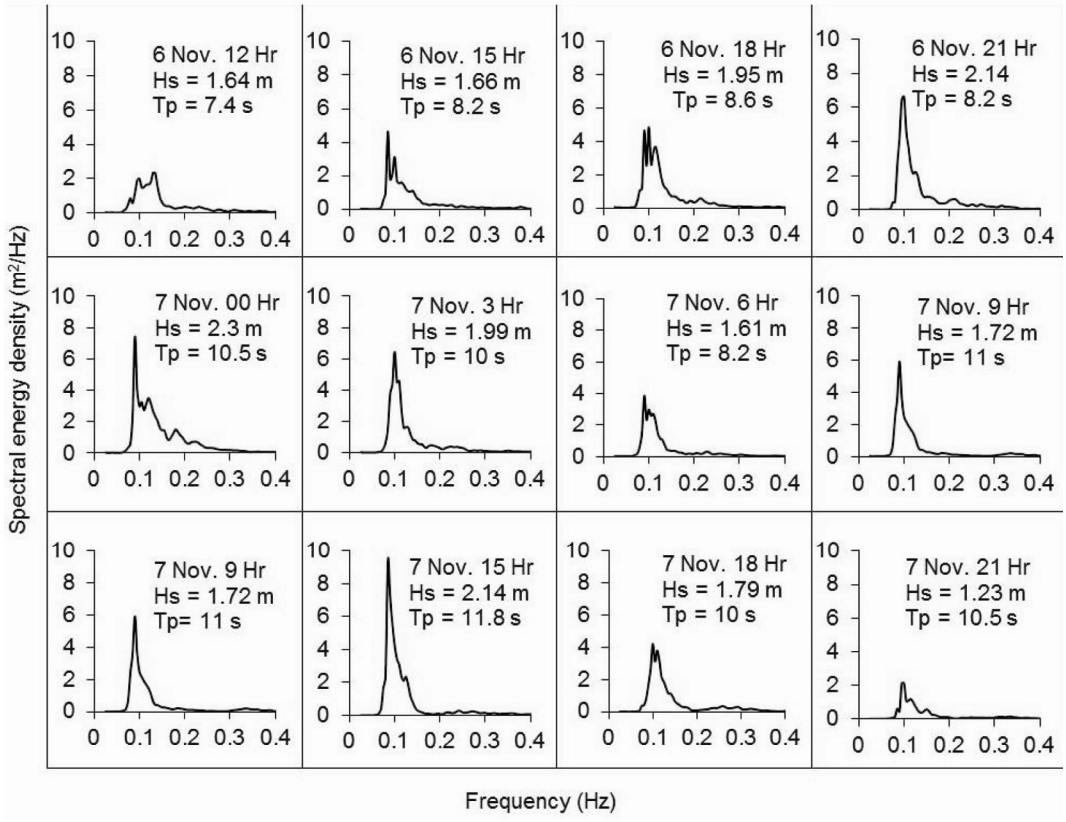

Figure 4. Typical wave spectra observed during *Jal* severe cyclonic storm (6 November 2010, 1200 h to 7 November 2010, 2100 h at 3 h intervals).

Figure 2 also shows the distribution of zero crossing periods (T_z). The periods have a narrow range (2–6 sec) during pre-monsoon and wide range (2–8 sec) during SW and NE monsoon months. During pre-monsoon period, nearly 66% occurs in 2–4 sec and 33% in 4–6 sec. During SW monsoon, T_z in the range 4–6 sec contributes nearly 74% of the distribution; 14% is in the range 2–4 sec; and 12% is in the range 6–8 sec. During NE monsoon, 73% of T_z distribution is in the range 4–6 sec; 19% in the range 2–4 sec; and 8% is in the range 6–8 sec. This distribution of T_z clearly indicates that pre-monsoon waves are dominated by short-period sea waves.

The peak period ranges from 2.1 to 20 sec with an average of 8.6 sec and standard deviation of 2.9 sec. Figure 2 shows the distribution of peak period. During SW monsoon, T_p ranges from 3 to 18.2 sec (with an average of 10.1 sec), 81% of the waves falls within the range (8–12 sec). Pre-monsoon peak wave periods are evenly distributed in the wave group range 0–4, 4–8 and 8–12 sec, within the range 2.1–20 sec. The average wave period during this period is only 7.1 sec; this may be due to the dominance of wind sea during pre-monsoon period over nearshore area. The peak period distribution during NE monsoon mainly ranges from 4 to 8 sec (48%) and 8 to 12 sec (43%), and for the rest of the waves more than 12 sec. The results of the study show that pre-monsoon peak wave period is dominated by short-period sea waves, SW monsoon by intermediate waves (combination of sea and swell) and NE monsoon by a combination of short, intermediate and long swells.

The seasonal average wave directions for pre-monsoon, SW monsoon and NE monsoon are 124°, 134° and 99° respectively. The dominant wave directions for pre-monsoon are ESE (59%) and SE (28%); SW monsoon are SE (78%) and SSE (22%); and NE monsoon are ENE (48%) and ESE (41%) respectively (Figure 2). The seasonal reversal of wave direction is not clearly understood from the total wave direction distribution. Hence, splitting of the total wave spectrum into sea and swell components is done.

The observed maximum spectral energy density varies between 0.01 and 14.26 m^2/Hz. During pre-monsoon, E_{max} varies between 0.02 and 9.1 m^2/Hz (with average value of 0.36); during SW monsoon the range falls within 0.01–4.8 m^2/Hz (with average value of 0.63 m^2/Hz); and during NE monsoon the range is 0.05–14.26 m^2/Hz (with average value of 1.04 m^2/Hz). The high value of E_{max} observed during NE monsoon may be due to prevalent rough conditions over the sea because of cyclones. Regression analysis showed a correlation coefficient of 0.81 and 0.96 between H_s, and observed E_{max} as well as H_s and estimated $E_{max} = 1.55*H_s^2$ respectively (Figure 3), compared with 0.82 for the entire years data collected along the east coast of India[8] and Gopalpur coast, Odisha[5].

Among the three major cyclones which developed along BoB, the impact of cyclone *Jal* was well experienced and recorded in the buoy, due to its close landfall along the Tamil Nadu coast. Figure 4 presents the observed wave spectra recorded at 3 h interval during 6–7 November 2010. The wave spectrum was flat and double-peaked in the initial stage of the cyclone (6 November 12 h UTC); then it became single-peaked when the cyclone approached mainland and made its landfall on 7 November 2010 at 15 h. The maximum spectral energy of 9.5 m^2/Hz was recorded on 7 November 2010 at 15 h (Figure 4). The observed H_s and H_{max} prior to the cyclone landfall were 2.14 and 5.7 m respectively. During the same period, the recorded H_s and H_{max} were 2.5 m and 4.7 m respectively along, the shallow water of Gangavaram[7]. After the cyclone landfall, the wave spectrum became flat with broader frequency range, lower wave height and energy. The effect of cyclone *Jal* was well-experienced along coastal Andhra Pradesh and Tamil Nadu. The storm-induced surge by cyclone *Jal* and severe flooding near its landfall killed 63 people in Andhra Pradesh and two in Tamil Nadu, with loss of property worth Rs 274 million and destruction of about 0.2 million houses along the coastal states[16].

The wave spectra were broader in shape with variation in spectral peakedness parameter (Q_p) between 1.05 and 3.98, and spectral width parameter (ε) between 0.53 and 0.84 respectively. Throughout the year, the directional spreading of sea waves was high (>40°) and swell waves was low (<15°) due to predominant swell direction. The observed higher value of directional spreading angle and spectral width decreased the spectral energy, leading to multi-peaked and multi-directional wave spectrum. This caused low wave spectral energy along the Cuddalore coast.

Figure 5 is a plot of the significant wave height (H_s, H_{sw} and H_{ss}). The range of H_s varied from 0.14 to 2.78 m. The maximum of H_{sw} and H_{ss} was recorded as 1.47 and 2.14 m respectively. Among the five extreme events (three cyclones and two low pressures) during the observation period, a maximum wave height (H_{max}) of 5.7 m was recorded during cyclone *Jal*[16]. The swell wave height (H_{ss}) exceeded more than 1 m during extreme events only; it was less than 0.5 m during January to April. The dominance (above 50% in wave height) of sea and swell waves over total H_s was analysed. Annually, 76% of waves is dominated by sea and 24% by swell. The sea waves are dominant (above 90%) during November to

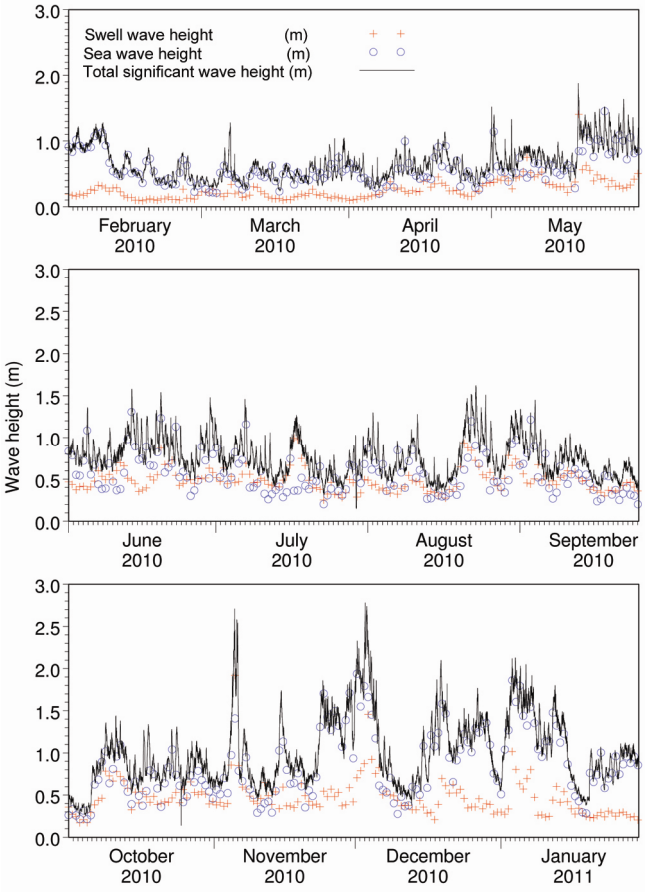

Figure 5. Time-series plots of sea, swell and total significant wave heights for pre-monsoon (top), SW monsoon (middle) and NE monsoon (down) periods.

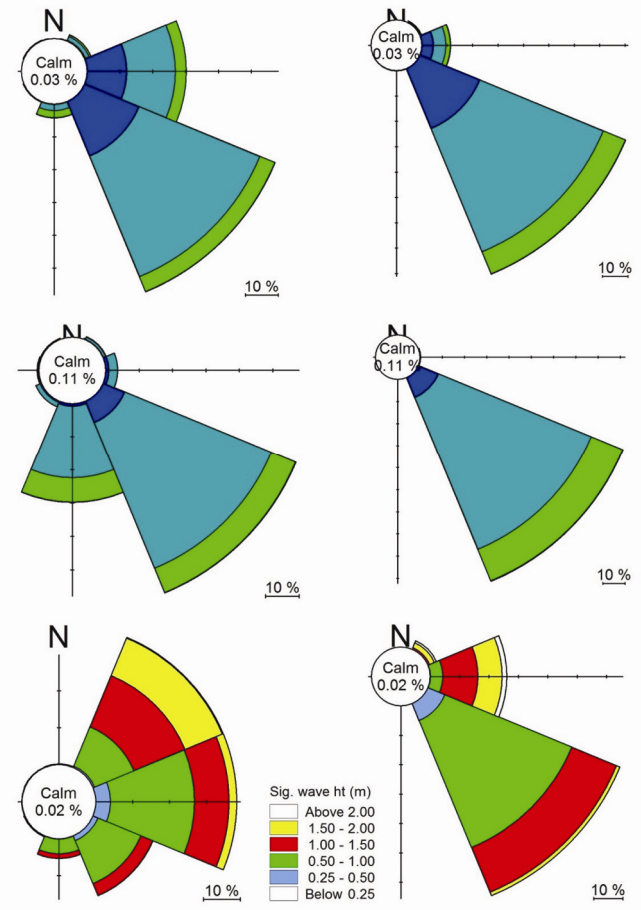

Figure 6. Rose diagram for sea and swell waves for pre-monsoon (top), SW monsoon (middle) and NE monsoon (down) periods.

May, swells during cyclonic events and mixed sea state during June to October. Similar studies conducted along the Gulf of Mannar showed 55.5% of the waves dominated by sea and 45.5% by swell waves annually[11], and 30% of the waves by sea and 70% by swell waves annually along the west coast[12]. The contribution of swell to the total H_s was 63.2% and sea was 36.8% along Visakhapatnam coast during June to September[10]. Regression analysis showed good positive correlation of 0.94 between H_s and H_{sw}, compared to 0.65 between H_s and H_{ss}. This result confirms that the magnitude of the significant wave height of the study area is dominated by sea waves.

The range of T_z of seas was from 3.54 to 7.67 sec with average value of 5.06 sec, mean T_{sw} and T_{ss} values were 4.02 and 10.12 sec respectively. The measured H_s was closely distributed over the periods 3–5 sec for T_{sw}, 3–7 sec for T_z and scattered between 9 and 13 sec for T_{ss}. Scattered distribution of H_s and T_{ss} may be due to increase in swell wave period by long swells during southwest monsoon and extreme events.

A distinct shift in sea wave direction of about 90° was observed during the periods 26 May–24 September 2010 and 27 October 2010–25 February 2011. The predominant swell direction was 135°, i.e. southeast (SE) throughout the year. The average sea wave direction during pre-monsoon (March–May), SW monsoon (June–September) and NE monsoon (October–January) was 135° (SE), 160° (SSE) and 75° (ENE) respectively (Figure 6). The sea and swell waves were recorded arriving from the same direction (135°) during pre-monsoon.

The study of wave characteristics off Cuddalore is different from other parts of the northern BoB due to obstruction of long swells by Sri Lanka mainland from the south Indian Ocean. Annually, the wind sea wave is dominant (76%), compared to swell waves. The distribution of wave height and wave period shows a linear relationship between H_s with T_{sw} and T_z, and scattered with T_{ss}. The shift in sea wave direction by 90° is observed between SW and NE monsoon, due to change in wind pattern over the Indian subcontinent and north Indian Ocean, while the predominant swell direction remains at 135°, i.e. SE throughout the year. This phenomenon is ubiquitous along the east coast of India[17]; the beaches are depositional during NE monsoon and erosional during SW monsoon season[4,18,19].

1. Earle, M. D., Development of algorithms for separation of sea and swell. US National Data Buoy Center Technical Report MEC-87-153, 1984.
2. Semedo, A., Suselj, K., Ruthersson, A. and Sterl, A., A global view on the wind sea and swell climate and variability from ERA-40. *J. Climate*, 2011, **24**, 1461–1479.
3. Wang, W. D. and Hwang, P. A., An operational method for separating wind sea and swell from Ocean wave spectra. *J. Atmos. Oceanic Technol*., 2001, **18**, 2052–2062.
4. Sanil Kumar, V., Pathak, K. C., Pednekar, P., Raju, N. S. N. and Gowthaman, R., Coastal processes along the Indian coastline. *Curr. Sci*., 2006, **91**, 530–536.
5. Mishra, P., Patra, S. K., Ramana Murthy, M. V., Mohanty, P. K. and Panda, U. S., Interaction of monsoonal wave, current and tide and their impact on beach profiles – a case study at Gopalpur, east coast of India. *Nat. Hazards*, 2011, **59**, 1145–1159.
6. Johnson, G., Sanil Kumar, V. and Balakrishnan Nair, T. M., Monsoon and cyclone induced wave climate over the near shore waters off Puduchery, south western Bay of Bengal. *Ocean Eng*., 2013, **72**, 277–286.
7. Sanil Kumar, V., Dubhashi, K. K. and Balakrishnan Nair, T. M., Wave spectral characteristics off Gangavaram, East coast of India. *J. Oceanogr*., 2014, **70**, 307–321.
8. Sanil Kumar, V., Anand, N. M., Kumar, K. A. and Mandal, S., Multi peakedness and groupiness of shallow water waves along Indian coast. *J. Coastal Res*., 2003, **19**(4), 1052–1065.
9. Aboobacker, V. M., Vethamony, P., Sudheesh, K. and Rupali, S., Spectral characteristics of the nearshore waves off Paradip, India during monsoon and extreme events. *Nat. Hazards*, 2009, **49**(2), 311–323.
10. Suresh, R. R. V., Annapurnaiah, K., Reddy, K. G., Lakshmi, T. N. and Balakrishnan Nair, T. M., Wind sea and swell characteristics off east coast of India, during southwest monsoon. *Int. J. Oceans Oceanogr*., 2010, **4**, 35–44.
11. Gowthaman, R., Sanil Kumar, V., Dwarakish, G. S., Mohan, S. S., Jai Singh and Ashok Kumar, K., Waves in Gulf of Mannar and Palk Bay around Dhanushkodi, Tamil Nadu, India. *Curr. Sci*., 2013, **104**(10), 1431–1435.
12. Aboobacker, V. M., Rashmi, R., Vethamony, P. and Menon, H. B., On the dominance of pre-existing swells over wind seas along west coast of India. *Cont. Shelf Res*., 2011, **31**, 1701–1712.
13. Catalogue of Indian Charts Electron Navigation Charts (ENCs) and Publications, National Hydrographic Office, Chart number-3003, Dehradun, 2012.
14. Datawell, B. V., *Datawell Wave Rider Reference Manual*, Datawell BV, The Netherlands, 2006.
15. Gilhousen, D. B. and Hervey, R., Improved estimates of swell from moored buoys. Proceedings of the 4th International Symposium WAVES 2001, ASCE: Alexandria, Virginia, USA, 2001, pp. 387–393.
16. Patra, S. K. and Jena, B. K., Wave characteristics during severe cyclonic storm Jal, along east coast of India. WMO International Conference on Indian Ocean Tropical Cyclones and Climate Change (IOTCCC-2012) New Delhi, WWRP 2013–04, 2012, pp. 152–159.
17. Patra, S. K. *et al.*, Cyclone and monsoonal wave characteristics of northwestern Bay of Bengal: long-term observations and modeling. *Nat. Hazards*, 2016, **82**, 1051–1083.
18. Ranga Rao, V., Ramana Murthy, M. V., Bhat, M. and Reddy, N. T., Littoral sediment transport and shoreline changes along Ennore on the southeast coast of India: field observations and numerical modelling. *Geomorphology*, 2009, **112**, 158–166.
19. Mohanty, P. K. *et al.*, Impact of groins on beach morphology: a case study near Gopalpur Port, east coast of India. *J. Coastal Res*., 2012, **28**, 132–142.

ACKNOWLEDGEMENTS. The present study is a part of the ongoing research project 'Technical Criteria Atlas (TCA)' funded by the Ministry of Earth Sciences (MoES), New Delhi. We thank the Secretary, MoES, New Delhi, for the necessary funding support, and the Director, National Institute of Ocean Technology, Chennai for encouragement and support.

Received 13 January 2016; revised accepted 12 November 2016

doi: 10.18520/cs/v112/i10/2115-2121